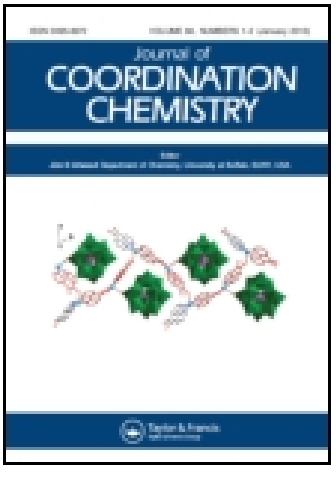

Journal of Coordination Chemistry
Publication details, including instructions for authors and subscription information:
http://www.tandfonline.com/loi/gcoo20

Mechanochemical synthesis and spectroscopic properties of 1,1′-ferrocenyldiacrylonitriles: the effect of para-substituents

Lucy M. Ombaka[a], Patrick G. Ndungu[a], Bernard Omondi[a] & Vincent O. Nyamori[a]

[a] School of Chemistry and Physics, University of KwaZulu-Natal, Durban, South Africa

Accepted author version posted online: 05 Jun 2014.Published online: 03 Jul 2014.

To cite this article: Lucy M. Ombaka, Patrick G. Ndungu, Bernard Omondi & Vincent O. Nyamori (2014) Mechanochemical synthesis and spectroscopic properties of 1,1′-ferrocenyldiacrylonitriles: the effect of para-substituents, Journal of Coordination Chemistry, 67:11, 1905-1922, DOI: 10.1080/00958972.2014.931946

To link to this article: http://dx.doi.org/10.1080/00958972.2014.931946

Journal of Coordination Chemistry, 2014
Vol. 67, No. 11, 1905–1922, http://dx.doi.org/10.1080/00958972.2014.931946

Mechanochemical synthesis and spectroscopic properties of 1,1′-ferrocenyldiacrylonitriles: the effect of *para*-substituents

LUCY M. OMBAKA, PATRICK G. NDUNGU, BERNARD OMONDI and VINCENT O. NYAMORI*

School of Chemistry and Physics, University of KwaZulu-Natal, Durban, South Africa

(*Received 18 November 2013; accepted 1 May 2014*)

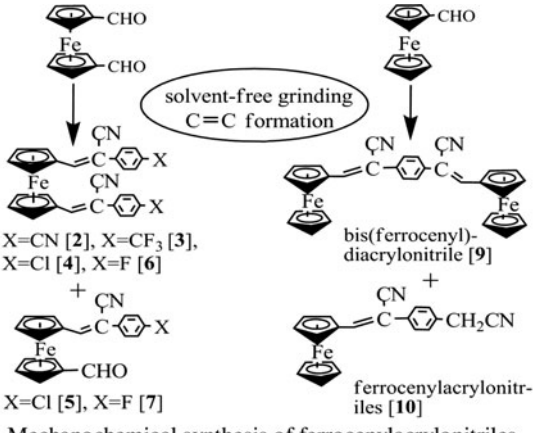

Mechanochemical synthesis of ferrocenylacrylonitriles.

An efficient and simple solvent-free mechanochemical approach for the synthesis of 1,1′-ferrocenyldiacrylonitriles was achieved by grinding together 1,1′-ferrocenedicarboxaldehyde (**1**) and phenylacetonitriles. A range of 1,1′-ferrocenyldiacrylonitriles and ferrocenylacrylonitriles (**2**–**7**) were synthesized within short reaction times, with water as the only by-product. In a similar manner, grinding together ferrocenemonocarboxaldehyde (**8**) and phenylenediacetonitrile yielded phenylene-3,3′-*bis*-(ferrocenyl)diacrylonitrile (**9**) and 3-ferrocenyl-2-(acetonitrophenyl)acrylonitrile (**10**). The yield and selectivity towards formation of ferrocenyldiacrylonitriles was strongly influenced by the electronegativity of the *para*-substituent on the phenyl ring of phenylacetonitriles. The compounds were characterized using NMR, IR, and UV–visible spectroscopy and HR-MS. Cyclic voltammetry measurements of selected compounds highlighted the role of ligands in tuning the electrochemical properties of 1,1′-ferrocenyldiacrylonitriles. X-ray crystallographic analysis highlighted the effect of the electronegativity of the *para*-substituent on the conformation of cyclopentadienyl rings attached to a ferrocenyl moiety.

*Corresponding author. Email: nyamori@ukzn.ac.za

Keywords: 1,1′-Ferrocenyldiacrylonitriles; 1,1′-Ferrocenedicarboxaldehyde; Solvent-free; Green chemistry; Mechanochemical

1. Introduction

Solvent-free synthesis of compounds is a growing research field in the quest for greener synthetic processes [1]. Mechanochemical synthesis of organometallic compounds, under solvent-free conditions, is of particular interest since a number of reactions can occur in the solid state [2], thereby eliminating the use of toxic solvents and reducing the overall cost of the synthesis [1]. Compared to reactions in solvents, solvent-free reactions take a shorter reaction time, exhibit higher atom economy, and allow for easier product isolation [3]. Although, numerous synthetic procedures used to synthesize compounds have been explored under solvent-free conditions [4], they remain relatively unexploited in the synthesis of ferrocenyl derivatives.

Mono- and di-substituted ferrocenyl derivatives containing substituted phenyl rings are good examples of ferrocenyl derivatives that can be synthesized via a solvent-free approach. In these compounds, the ferrocenyl moiety is an electron donor while the attached ligand is a π-electron acceptor. Such ferrocenyl derivatives are potential new materials with desirable properties for application in various fields. They could be useful in fluorescence [5], nonlinear optical devices [6], electron transfer processes [7], electrochromic devices [8], medicinal applications [9] and even as catalysts in the synthesis of shaped carbon nanomaterials such as carbon nanotubes (CNTs) [10]. Research geared towards the synthesis of nitrogen-doped carbon nanotubes (N-CNTs) using nitrogen-containing organometallic compounds as catalysts is of interest [11–13]. The incorporation of nitrogen into the graphene structure of CNTs (i.e. doping CNTs with nitrogen) has been reported to enhance both the electronic and physical properties of CNTs [14]. Hence, nitrogen-containing ferrocenyl derivatives such as 1,1′-ferrocenyldiacrylonitriles are potential organometallic catalysts for the synthesis of N-CNTs.

Under mechanochemical conditions, di- and mono-substituted ferrocenyl derivatives can be synthesized from condensation of 1,1′-ferrocenedicarboxaldehyde and ferrocenemonocarboxaldehyde, respectively, with other compounds. For example, 1,1′-ferrocenyldiimines were synthesized from the condensation of 1,1′-ferrocenedi-carboxaldehyde and aromatic amines [15], while ferrocenylimines were synthesized by the condensation of ferrocenemonocarboxaldehyde and aromatic amines [16]. Similarly, *bis*-ferrocenylethenes and *bis*-ferrocenylimines have been synthesized by condensation of ferrocenemonocarboxaldehyde with phosphonium salts [17] and diaminoalkanes [18], respectively.

Although the mechanochemical reactions of 1,1′-ferrocenedicarboxaldehyde have been reported [15], the synthesis of 1,1′-ferrocenyldiacrylonitriles, in particular, has not yet been reported. In this study, a simple and efficient solvent-free procedure for synthesis of 1,1′-ferrocenyldiacrylonitriles and *bis*-ferrocenyldiacrylonitrile was achieved by mechanochemical grinding of solid reactants to obtain the desired product. Additionally, the spectroscopic, electrochemical, and X-ray crystallographic analyses of selected compounds are also discussed.

2. Results and discussion

2.1. *Synthesis of 1,1′-ferrocenyldiacrylonitriles*

Grinding together 1,1′-ferrocenedicarboxaldehyde **1** and substituted phenylacetonitriles in the presence of catalytic amounts of piperidine yielded a range of 1,1′-ferrocenyldiacrylonitriles (**2**, **3**, **4**, and **6**) and ferrocenylcarboxacrylonitriles (**5** and **7**) as depicted in scheme 1.

Different mole ratios of **1** : phenylacetonitrile (ca. 1 : 2 and 1 : 2.2) were used and it was noted that a mole ratio of 1 : 2.2 gave products in higher isolated product yields. Generally, the mixture containing the starting materials readily turned into a melt or a gum upon grinding at ambient temperatures. The obtained melt or gum was dried under vacuum, and IR and ^{1}H NMR spectroscopy were used to confirm reaction completion. Formation of 1,1′-ferrocenyldiacrylonitriles was marked by disappearance of a sharp IR absorption band at ≈1650 cm^{-1} (CHO) and the appearance of a strong nitrile absorption at ≈2200 cm^{-1}. From ^{1}H NMR spectra, the formation of 1,1′-ferrocenyldiacrylonitriles was marked by the disappearance of a carbonyl proton resonance peak (≈10 ppm) and the appearance of an ethylene proton resonance peak (≈7.4 ppm).

The synthesis of 1,1′-ferrocenyldiacrylonitriles involved two mechanistic steps (scheme 2). First, the methylene carbon on the phenylacetonitriles was deprotonated by piperidine. Second, a Knoevenagel condensation occurred between the anionic methylene carbon and the carbonyl carbon [19].

Selectivity towards ferrocenyldiacrylonitrile formation showed a dependence on the electronegativity of the *para*-substituent on the phenyl rings. For example, *para*-substituted phenyl rings containing more electronegative groups (CN and CF_3) selectively formed only 1,1′-ferrocenyldiacrylonitriles (**2** and **3**) as depicted in table 1. In contrast, the relatively less electronegative substituents (Cl and F) in the *para*-position of the phenyl ring formed both 1,1′-ferrocenyldiacrylonitriles (**4** and **6**) and ferrocenylcarboxyacrylonitriles (**5** and **7**). This could imply that more electronegative groups stabilize the deprotonated methylene intermediate (scheme 2) more than the relatively less electronegative groups leading to selective formation of 1,1′-ferrocenyldiacrylonitriles. The stronger electronegative substituents (CN and CF_3) also gave larger isolated product yields compared to relatively less electronegative substituents (Cl and F). The higher isolated yields (74–78%) were comparable to those of similar compounds synthesized from 1,1′-ferrocenedicarboxaldehyde in solvents [20, 21].

Interestingly, the *para*-Cl substituted phenylacetonitrile formed ferrocenyldiacrylonitrile (**4**) as the major product, while the *para*-F equivalent did not form ferrocenyldiacrylonitrile (**6**) as the major product (table 1). This observation may suggest that the *para*-Cl substituent was more reactive than the *para*-F substituent. It is plausible that the activity difference of

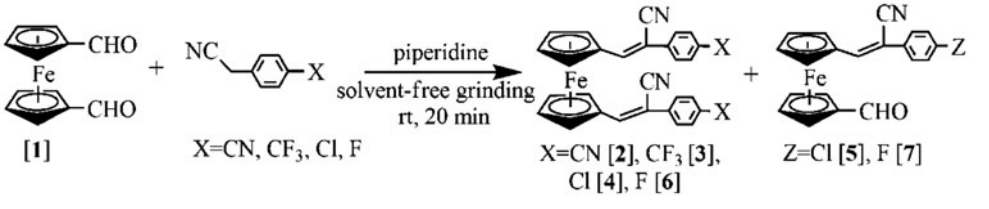

Scheme 1. Mechanochemical synthesis of 1,1′-ferrocenyldiacrylonitriles and ferrocenylcarboxacrylonitriles under solvent-free conditions.

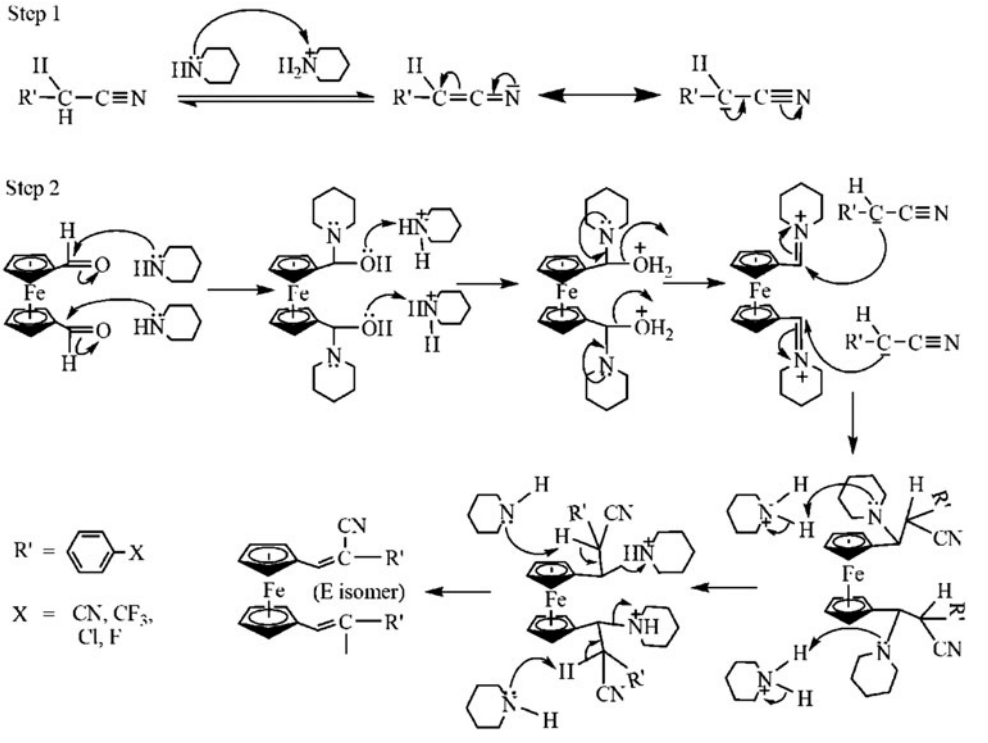

Scheme 2. Plausible reaction mechanism for formation of 1,1′-ferrocenyldiacrylonitriles.

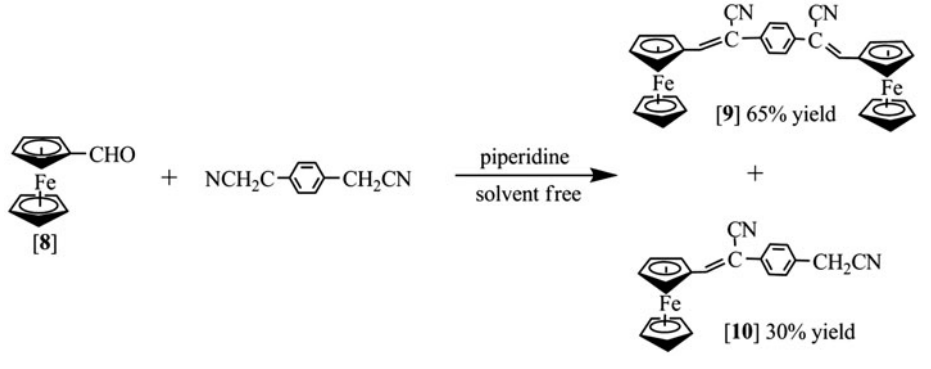

Scheme 3. Mechanochemical reactions of **8** and phenylenediacetonitrile under solvent-free conditions.

para-Cl and -F substituents may be attributed to the electronegativity dipole and resonance dipole of chlorine versus fluorine when attached to a phenyl carbon [15]. Fluorine is more electronegative than chlorine and has an efficient 2p orbital that overlaps with carbon resulting in a strong resonance dipole, however, the two dipoles cancel out leading to a net dipole of zero [22]. In the case of the chlorine substituent, with inefficient 3p–2p orbital overlap with carbon (thus resulting in a weak resonance dipole), the electronegativity dipole

Table 1. Isolated yields of 1,1′-ferrocenyldiacrylonitriles and ferrocenylacrylonitrile.*

Compound	*Para*-substituent	Yield (%)
2	CN	74
3	CF_3	78
4	Cl	52
5	Cl	10
6	F	7
7	F	24

*Isolated yields based on **1** as the limiting reagent.

dominates over the resonance dipole leading to a net electron-withdrawing effect. Hence, the *para*-Cl substituent on the phenyl ring could give a more stable intermediate, which leads to better selectivity towards 1,1′-ferrocenyldiacrylonitrile formation, and higher isolated yields than for the *para*-F substituent.

2.2. *Mechanochemical reactions of ferrocenemonocarboxaldehyde and phenylenediacetonitrile*

Bis-metallocenyl compounds can be synthesized by attaching two metallocenyl moieties to a bidentate ligand or addition of another metallocene to a monodentate metallocenyl derivative. For example, Braga *et al.* [23] reported the synthesis of *bis*-ferrocenyl complexes by reacting ferrocenyl derivatives with transition metal salts. In this report, we utilize a mechanochemical approach to attach two ferrocenyl moieties to a bidentate ligand (phenylenediacetonitrile). Grinding together ferrocenemonocarboxaldehyde **8** and phenylenediacetonitrile in the presence of 1–2 drops of piperidine, and at ambient temperatures, gave phenylene-3,3′-*bis*-(ferrocenyl)diacrylonitrile **9** and 3-ferrocenyl-2-(acetonitrophenyl)-acrylonitrile **10** (scheme 3).

To determine whether the reactions leading to formation of **9** and **10** were complete, ^{1}H- and ^{13}C NMR spectroscopy was used. From the ^{1}H NMR spectrum, formation of **9** was marked by the disappearance of a carbonyl proton resonance (≈10 ppm) and the appearance of an ethylene proton resonance (≈7.43 ppm). Similarly, formation of **10** was marked by the disappearance of a carbonyl proton resonance (≈10 ppm) and the appearance of an ethylene proton resonance (≈7.59 ppm) and a methylene resonance peak (≈3.75 ppm). From the ^{13}C NMR spectrum, the conspicuous absence of a strong carbonyl carbon resonance (≈190 ppm) marked the formation of either **9** or **10**.

To optimize the reaction conditions, different mole ratios of **8** : phenylenediacetonitrile (ca. 1 : 1, 1.4 : 1 and 2 : 1) were used. Among the three sets of mole ratios used, a mole ratio of 1.4 : 1 gave the highest yield. Since phenylenediacetonitrile was the limiting reagent, a mole ratio of 1.4 : 1 that contains an excess of phenylenediacetonitrile resulted in higher conversions of **8–9** and **10**. In all cases, the major product obtained was **9** while the minor product was **10**. Generally, the reaction occurred within 5–10 min of grinding. This could imply that under solvent-free conditions, phenylenediacetonitrile is less reactive than phenylacetonitrile which immediately reacts with **8** at room temperature [15]. Longer reaction times (≈20 min) favored production of **9**, while shorter reaction times (≈5 min) yielded almost equivalent quantities of **9** and **10**. Thus, longer reaction periods allow for greater conversion of **10–9** until a steady-state condition reaction is attained.

2.3. *UV–visible spectroscopy*

UV–visible absorption spectra of selected compounds are shown in figure 1 and the peak absorption data are summarized in table 2. All compounds exhibit absorptions in the UV and visible regions attributed to π–π^* ligand-centered transitions and metal–ligand centered transitions, respectively [24]. A shoulder was observed in the absorption spectra of di-substituted 1,1′-ferrocenyldiacrylonitriles (**2**, **3**, and **4**, i.e. 313, 301, and 302 nm, respectively, table 2 and figure 1). In **10** and related mono-substituted ferrocenylacrylonitriles [15], similar shoulders were not observed. This could imply that electronic interactions occur between the two ligands attached to a single ferrocenyl moiety in di-substituted 1,1′-ferrocenyldiacrylonitriles. Substitution of the ferrocenyl electron donor with phenylacrylonitriles resulted in a significant red-shift of the absorption peaks. Comparison of **2**, containing a more electronegative *para*-substituent, with **4**, containing a less electronegative *para*-substituent, shows that **2** is more red-shifted than **4** (table 2). This implies that stronger electron-withdrawing groups on the phenyl *para*-position increase the electronic interactions between the ligands and the ferrocenyl moiety metal center, resulting in a greater red-shift [25]. A comparison of **2**, containing one ferrocenyl moiety, and **9**, containing two ferrocenyl moieties, shows that **9** has a larger red-shift. Compound **9**, that exhibited a strong absorption in the UV region, has previously been reported for application in optical recording materials [26]. Thus, **2** which showed a more intense absorption in the UV region can be investigated for possible applications in optical recording materials.

The solvatochromic behaviors of **2**, **3**, and **4** were recorded in DMF, acetonitrile, and DCM (table 3). All three compounds exhibited a red-shift upon an increase of solvent

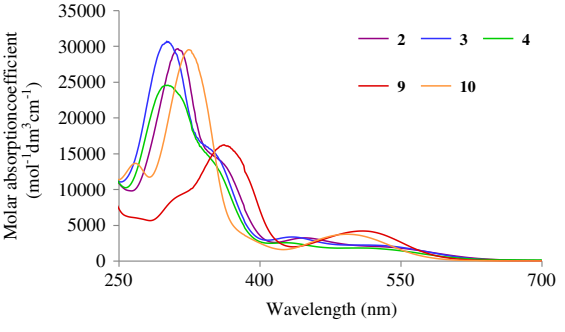

Figure 1. UV–visible spectra of **2**, **3**, **4**, **9**, and **10** in acetonitrile.

Table 2. Maximum absorption wavelength and corresponding molar absorption coefficients in acetonitrile.

Compound	λ_{max}/nm (ε_{max}/M^{-1} dm^3 cm^{-1})		
Ferrocene [23]	435(1276)	324(1120)	
2	514(2095)	447(3244)	313(29,679)
3	506(2244)	434(3367)	301(30,727)
4	505(1831)	427(2567)	302(24,572)
9	509(4206)	362(16,251)	
10	494(3753)	324(29,537)	

Table 3. Maximum absorption wavelength of selected 1,1′-ferrocenyldiacrylonitriles in DMF, dichloromethane, and acetonitrile.

	λ_{max}/nm		
Compound	DMF	DCM	Acetonitrile
2	491	454	447
	319	317	313
3	469	436	434
	310	304	301
4	460	428	427
	355	313	302

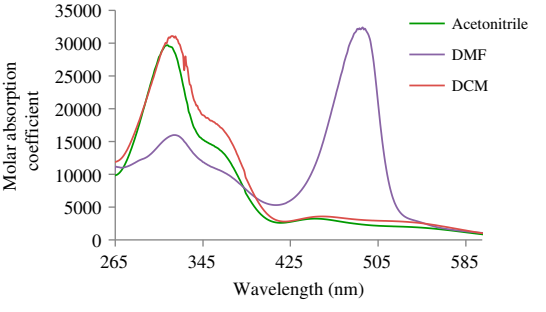

Figure 2. UV–visible spectra of **2** in acetonitrile, DMF, and dichloromethane.

polarity with **2** showing the greatest shift (figure 2). Thus, the electronegativity of the phenyl *para*-substituent influenced the dispersion interactions and the dipole-dipole interactions between the compounds and solvents [27]. Since all three compounds exhibited solvatochromic behavior, they are potentially useful for nonlinear optical studies [28].

2.4. *Cyclic voltammetry*

The redox potentials of selected compounds (table 4) showed a reversible or quasi-reversible [29] redox process within a potential range of $E_{p½} = 600–850$ mV. Reversibility was taken to imply that the peak potential separation ($\Delta E_P = E_{pa} - E_{pc}$) was 80 mV or less, and that the peak current ratio (i_{pa}/i_{pc}) was approximately one.

Table 4. Redox potentials of ferrocene and selected 1,1′-ferrocenyldiacrylonitriles.

Compound	E_{pa} (mV)	E_{pc} (mV)	ΔE_p (mV)	$E_{p_2^1}$ (mV)
Ferrocene [15]	516	401	115	459
2	859	818	41	839
3	879	798	81	839
4	834	763	71	799
9	718	582	136	650
10	657	592	65	624

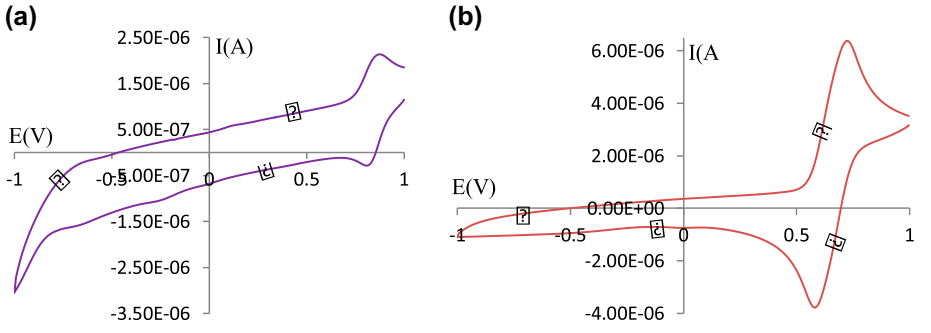

Figure 3. Cyclic voltammograms of (a) **2** and (b) **9** at a platinum working electrode, silver/silver chloride reference electrode, and at a scan rate of 100 mV s^{-1} in acetonitrile.

A single reversible or quasi-reversible oxidation peak (figure 3) was observed associated with ferrocenium–ferrocene oxidation (Fc^{+}/Fc) [30]. A positive shift of the ferrocenyl redox potential was noted for substituted ferrocenyl compounds compared to free ferrocene [31].

A comparison of **2** and **4**, which differ only in their phenyl *para*-substituent, shows that *para*-CN caused a more positive shift in the redox potential of the ferrocenyl moiety compared to *para*-Cl. This implies that, as the electronegativity of the *para*-substituent increases, the positive charge on iron increases making the ferrocenyl moiety harder to oxidize [32].

Compound **2**, containing two ligands on one ferrocenyl moiety, showed a more positive redox potential than **9** which has two ferrocenyl moieties attached to one ligand. Thus, attaching two ligands onto one ferrocenyl moiety increased the donor–acceptor coupling, making it harder to oxidize the ferrocenyl moiety [33]. This can also be attributed to a stronger electron-withdrawing effect of the ligands on the ferrocenyl moiety in **2** than in **9** [34]. Compounds **2**, **9**, and **10** showed different redox peak separation values ($\Delta E_P = E_{ps} - E_{pc}$), indicating that the electron transfer processes and HOMO–LUMO gaps can be influenced by the number of π-acceptor ligands attached to the ferrocenyl moiety. Compound **2** has a lower ΔE_p value (41 mV) compared to that of **9** (136 mV). This could suggest that, attaching two π-electron-acceptors to one ferrocenyl moiety (**2**) increases the electron transfer process while, attaching two ferrocenyl moieties to a single π-electron-acceptor depresses the electron transfer process. Consequently, **9** can be studied further for applications in electron transfer processes such as molecular switches [33].

2.5. *X-ray crystallography*

The molecular structures of **2** and **4** are shown in figure 4(a) and (b), respectively, along with the atom numbering scheme. Selected bond distances and angles are compared in table 5. The two compounds are isomorphous; the difference being mainly in the β angle of 119.733(3)° in **2** and 108.902(4)° in **4**. The molecular structure of **2** features two cyanoethyl benzonitrile groups attached to two cyclopentadienyl rings of the ferrocenyl moiety in a slightly twisted fashion as opposed to the energetically favored *trans* conformation. In the structure of **4**, a Cl replaces both the *p*-cyano groups but also maintains the *cis* conformation.

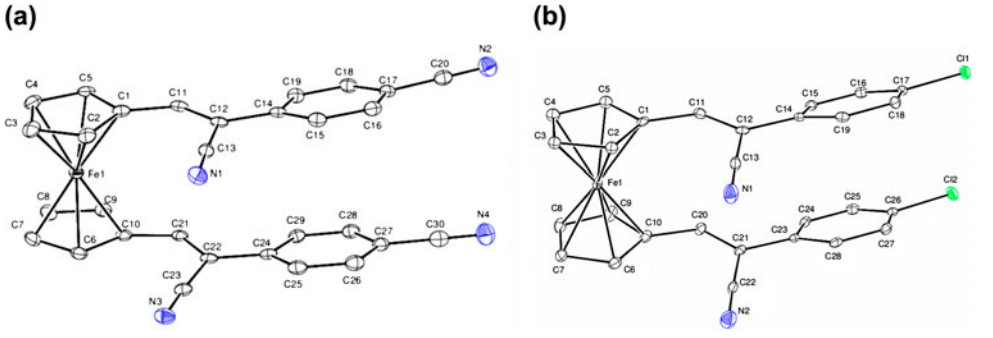

Figure 4. ORTEP diagram along with the atom-numbering scheme for (a) **2** and (b) **4**. Ellipsoids are drawn at 50% probability level. Hydrogens have been omitted for clarity.

The *para*-substituents play a role in the conformations of the cyclopentadienyl rings of the two compounds where in **2** they are staggered by 15.85(3)° from an ideal eclipsed geometry while in **4**, they have an eclipsed geometry, twisted only by an average of 0.654 (2)°. The electron-withdrawing effect of the cyano group is greater than that of the chloro substituent and therefore there is a greater decrease in the π-stacking ability of the aromatic moieties. Furthermore, the $\pi \ldots \pi$ distance of 3.644(3) Å between the phenyl rings of the benzonitrile moiety is considerably longer than that between the chlorobenzyl moieties in **4** of 3.570(3) Å. Since the substituted phenyl rings have short $\pi \ldots \pi$ distances, it therefore indicates that electrostatic and inductive effects appear to be more important [35]. For **2**, repulsive interactions dominate. There is low planarity between the cyclopentadienyl rings and the substituted phenyl rings attached to them; the planarity is slightly better in **2** than in **4**. All Fe–C bond distances and angles are within the expected ranges of similar ferrocene derivatives [36].

ORTEP drawings for **9** and **10** are shown in figure 5(a) and (b), respectively, along with the atom-numbering scheme. Selected bond distances and angles are compared in table 6. The molecular structure of **9** consists of two ferrocenyl units connected by a substituted 2-phenylacrylonitrile ligand. The configuration around the substituted 2-phenylacrylonitrile ligand is *trans*; the planes of the substituted cyclopentadienyl rings and the plane of the phenyl ring are unsymmetrical with dihedral angles of 28.11(7)° on one end and 42.95(6)°

Table 5. Selected bond lengths (Å) and angles (°) for **2** and **4**.

	2	**4**		**2**	**4**
C–C_{Cp}	1.448(3)	1.453(5)	C–C_{Cp}	1.449(3)	1.445(5)
C=C	1.355(3)	1.359(5)	C=C	1.353(3)	1.349(5)
C–C_{Ph}	1.485(3)	1.492(5)	C–C_{Ph}	1.483(3)	1.490(5)
C_{Cp}–C=C	128.85(17)	128.7(4)	C_{Cp}–C=C	130.78(17)	128.3(4)
C=C–C_{Ph}	124.74(16)	122.6(4)	C=C–C_{Ph}	123.67(17)	122.2(4)
C=C–C_N	120.65(17)	121.8(4)	C=C–C_N	121.04	121.8(4)
C_{Ph}–C–C_N	114.59	115.6(3)	C_{Ph}–C–C_N	115.29	116.0(3)
C=C–C_{Ph}–C_{Ph}	165.86(18)	156.3(4)	C=C–C_{Ph}–C_{Ph}	164.22(18)	154.0(4)

Note: C_{Cp} means a carbon on a cyclopentadienyl ring; C_{Ph} means carbon on a phenyl ring; C_N means a carbon on a cyano group.

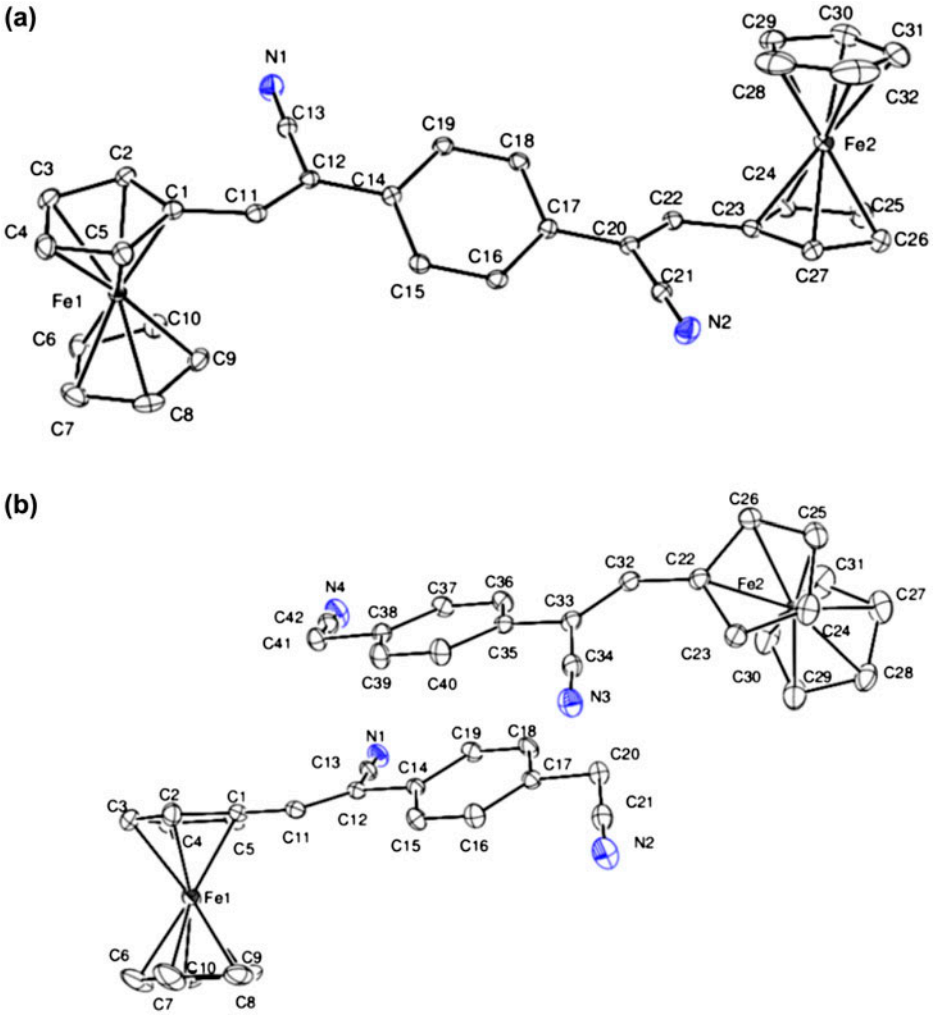

Figure 5. ORTEP diagram along with the atom-numbering scheme for (a) **9** and (b) **10**. Ellipsoids are drawn at 50% probability level. Hydrogens have been omitted for clarity.

on the other, meaning therefore that the molecule belongs to a C_1 point group. In addition, whereas one of the ferrocenyl moieties adopts a twisted conformation (small staggering angle of 2.12°), the other adopts an ideal staggered conformation (staggering angle of 45.99°). This lack of planarity is seen in the reduced π-conjugation in the molecule and especially along the phenylene dipropenenitrile ligand. The cyclopentadienyl rings of each of the ferrocenyl moieties are planar with a tilt angle of approximately 1.8° in one and 1.4° in the other. Compound **10** crystallizes with two molecules in the asymmetric unit, $\mathbf{10_I}$ containing Fe1 and $\mathbf{10_{II}}$ containing Fe2. The two molecules are not related by symmetry given the different orientations of the ferrocenyl moieties.

The cyclopentadienyl rings in each of the two molecules are essentially planar with angles between the set of planes of each of the rings being 0.15° and 1.56° in $\mathbf{10_I}$ and $\mathbf{10_{II}}$,

Table 6. Selected bond lengths (Å) and angles (°) for **9** and **10**.

	9	**10_I**		**9**	**10_{II}**
C–C_{Cp}	1.449(2)	1.446(6)	C–C_{Cp}	1.448(2)	1.448(6)
C=C	1.353(2)	1.355(5)	C=C	1.349(3)	1.354(5)
C–C_{Ph}	1.481(2)	1.487(5)	C–C_{Ph}	1.481(2)	1.483(5)
C_{Cp}–C=C	129.75(16)	127.4(4)	C_{Cp}–C=C	129.36(16)	126.7(4)
C=C–C_{Ph}	124.40(15)	124.6(3)	C=C–C_{Ph}	123.32(15)	125.6(4)
C=C–C_N	120.30(16)	119.7(4)	C=C–C_N	120.67(16)	119.4(4)
C_{Ph}–C–C_N	115.22(15)	115.6(3)	C_{Ph}–C–C_N	116.01(15)	115.1(3)
C=C–C–C_{Ph}–C_{Ph}	−162.70(17)	−164.3(4)	C=C–C–C_{Ph}–C_{Ph}	150.73(17)	−163.4(4)

Note: C_{Cp} means a carbon on a cyclopentadienyl ring; C_{Ph} means carbon on a phenyl ring; C_N means a carbon on a cyano group.

Table 7. Hydrogen bonding geometry for **9** and **10** (Å/°).

C–H···N	C–H	H···N	C···N	<C–H···N	Symmetry operator
9					
C11–H11···N2	0.95	2.51	3.321(2)	143	$1-x, -y, 2-z$
C15–H15···N2	0.95	2.60	3.544(2)	170	$1-x, -y, 2-z$
C22–H22···N1	0.95	2.44	3.317(2)	154	$-x, -y, 1-z$
10					
C8–H8···N2	1.00	2.61	3.521(7)	152	$1-x, 1-y, 1-z$
C20–H20a···N1	0.99	2.40	3.321(5)	155	$1-x, -y, 1-z$
C30–H30···N4	1.00	2.44	3.399(7)	160	$2-x, 2-y, 1-z$
C32–H32···N1	0.95	2.49	3.365(5)	154	$x, 1+y, z$
C41–H41A···N3	0.99	2.40	3.322(5)	155	$2-x, 2-y, 1-z$

respectively. Each of the molecules has two sets of planes: the plane of the cyclopentadienyl rings [C1–C5 and C11, and C22–C26 and C32 in **10_I** and **10_{II}**, respectively] and the plane of the phenyl ring and the adjacent carbons [C14–C19 and C2 and C20; C35–C40 and C33 and C41 in **10_I** and **10_{II}**, respectively]. The nitrile groups project away from these two planes differently in each of the two molecules. In **10_I**, the angle between the two sets of planes is 36.82(13)° while in **10_{II}**, the same angle is 45.33(15)°. The cyclopentadienyl rings in the two ferrocenyl moieties adopt a slightly staggered geometry and have staggering angles that are different in the two molecules: 9.60° in **10_I** and 6.28° in **10_{II}**. Bond distances and angles do not show any significant differences between the two molecules and are comparable to **2** and **9**, as well as to those of related structures [37].

The lattice structures of **9** and **10** are dominated by a series of C–H···N intermolecular hydrogen bonds. In **9**, these hydrogen bonds link centrosymmetrically related molecules into chains that run diagonally across the crystallographic *bc* plane. In the crystal structure of **10**, the C–H···N hydrogen bonds connect molecules to form layered chains of molecules that run along the crystallographic *b*-axis (table 7).

3. Conclusion

The mechanochemical synthesis of 1,1′-ferrocenyldiacrylonitriles provided an efficient approach for a range of ferrocenyl compounds. The method yielded high to moderate

quantities of 1,1′-ferrocenyldiacrylonitriles depending on the electron-withdrawing group attached to the phenyl *para*-position. Selectivity towards ferrocenyldiacrylonitrile formation was favored by the presence of a strong electron-withdrawing group on the *para*-substituent of the phenyl rings. The reaction times were short and all compounds were conveniently isolated. Therefore, similar solvent-free procedures can be developed for synthesis of bimetallic compounds containing similar or different metal centers. Herein, we also demonstrate that by attaching an appropriate π-acceptor group to the ferrocenyl moiety it allows the optoelectronic properties of the ferrocenyldiacrylonitriles to be tuned. In addition, the donor–acceptor electronic interactions and electron transfer processes are enhanced when two π-acceptor ligands are attached to one ferrocenyl moiety. On the contrary, attaching two ferrocenyl moieties to a single π-acceptor reduced the electron transfer process. Hence, the redox behavior of 1,1′-ferrocenyldiacrylonitrles can be switched from reversible to irreversible by attaching an appropriate number of π-acceptor groups. The X-ray crystallographic analysis showed the different preferred solid state conformations of the ferrocenyl moiety in mono- and di-substituted ferrocenyldiacrylonitriles.

4. Experimental

4.1. *General chemicals and instrumentation*

Solvent-free reactions involving grinding of reactants were performed in the open air. All reactants were used as received. Solvents used in purification of compounds and for growing crystals were dried by using standard literature methods prior to use. Aluminum-backed silica gel 60 F_{254} plates were used to carry out thin-layer chromatography in solvents of varying polarity. Purification of products by column chromatography was accomplished by using silica gel 60, 0.063–0.2 mm. The melting points of various compounds were determined either by using a Bibby Stuart Scientific model SMP3 apparatus or by using a Shimadzu Differential Scanning Calorimeter (DSC 60) apparatus. Infrared spectroscopy was conducted on a Perkin Elmer Universal ATR Spectrum 100 FTIR spectrometer. ^{1}H and ^{13}C NMR spectra were recorded on a 400 MHz Bruker Ultrashield spectrometer at RT. For NMR spectroscopic analysis, samples were dissolved in deuterated chloroform and values were obtained relative to tetramethylsilane. Mass spectra of various compounds were obtained from an Agilent Technologies, 1100 series, ion-trap mass spectrometer. Electronic spectra were recorded in acetonitrile, dichloromethane, and DMF with a Perkin Elmer Lambda 35 UV–visible spectrophotometer with 10 mm path length quartz cuvettes. Cyclic voltammetry measurements were performed on a Metrohm ion analysis instrument with 757 VA Computrace software. A three-electrode configuration consisting of a rotating platinum disk working electrode rotating at 2000 rpm, platinum-wire auxiliary electrode and silver/silver chloride reference electrode was used. The voltammetry measurements were made in dry acetonitrile with 10^{-2} M tetrabutylammonium tetrafluoroborate as the supporting electrolyte. For the cyclic voltammetry measurements, 10 cm^3 of solution containing approximately 10^{-3} M of each compound was used. A scan rate of 100 mV s^{-1} was used and $E_{1/2}$ values were obtained by averaging the anodic and cathodic peak potentials.

4.2. *Synthesis of 1,1′-ferrocenyldiacrylonitriles compounds from 1,1′-ferrocenedicarboxaldehyde; general procedure*

The general procedure for synthesizing 1,1′-ferrocenyldiacrylonitriles was developed from that described by Imrie *et al.* [15]. Compound **1** (1 eq.) and substituted phenylacetonitriles (2.2 eq.) were mixed in a Pyrex tube fitted with a ground-glass joint. The compounds were thoroughly ground with a glass rod. One to two drops of piperidine was added into the Pyrex tube and the mixture was further ground at RT until a melt was formed. The Pyrex tube was sealed and placed in a shaker for approximately 20 min. To evaporate the remaining piperidine (boiling point 106 °C) and water formed as a by-product, the samples were first dried in open air, and thereafter under a vacuum line. The products were further purified by silica gel chromatography. The formation of the products was determined using IR or NMR spectroscopy (^{1}H and ^{13}C). In solid-state IR spectra, formation of the products was characterized by the disappearance of the sharp carbonyl absorption at approximately 1650 cm^{-1} and the appearance of a strong nitrile absorption at approximately 2200 cm^{-1}. ^{1}H and ^{13}C NMR spectra showed the disappearance of the carbonyl resonance and the appearance of alkene resonance peaks. Pure compounds were further analyzed by mass spectrometry, microanalysis, and X-ray diffraction.

4.2.1. Synthesis of 1,1′-ferrocenyldi[-2(4-cyanophenyl)acrylonitrile] (2). The general procedure described in Section 4.2 was followed by using 1,1′-ferrocenyldi-carboxaldehyde (**1**) (145.0 mg, 0.60 mM) and 4-cyanophenylacetonitrile (188.0 mg, 1.32 mM). Upon grinding a deep maroon paste was formed, which was dried to obtain a maroon solid. Reaction completion was monitored by using preparative TLC plates with a solvent system of hexane/diethyl ether (1 : 1), and the product was then purified by column chromatography with a solvent system of hexane/diethyl ether (1 : 1) to obtain the product as dark maroon crystals (219.0 mg, 74%) and 37.0 mg of 1,1′-ferrocenedicarboxaldehyde (**1**). d.p. ca. 325 °C; IR (cm^{-1}) 3182, 2926, 2852, 2213, 1608, 1587, 1510, 1452, 1417, 1371, 1319, 1251, 1180, 1035, 996, 918, 830, 819, 542, 501, 486, 456, 425; ^{1}H NMR spectra ($CDCl_3$) 7.55 (4H, d, *J* 8.4 Hz, ArH), 7.47 (4H, d, *J* 8.5 Hz, ArH), 7.34 (2H, s, CH), 5.08 (4H, s, C_5H_4), 4.65 (4H, s, C_5H_4); ^{13}C NMR spectra ($CDCl_3$) 132.7, 125.3, 77.2, 73.7, 72.2; HR-MS ($C_{30}H_{18}FeN_4$) ES: $[M + H^+]$ *m/z* Calcd 491.0959, found 491.0969.

4.2.2. Synthesis of 1,1′-ferrocenyldi[-2(4-{trifluoromethyl}phenyl)acrylonitrile] (3). The general procedure described in Section 4.2 was followed by using 1,1′-ferrocenyldi-carboxaldehyde (**1**) (145.0 mg, 0.60 mM) and 4-(trifluoromethyl)phenylacetonitrile (244.0 mg, 1.32 mM). Upon grinding a deep red paste was formed, which was dried to obtain a red solid. Reaction completion was monitored using preparative TLC plates with a solvent system of hexane/diethyl ether (1 : 1) and the product was then purified by column chromatography with a solvent system of hexane/dichloromethane (1 : 1) to obtain red crystals as the product (268.0 mg, 78%) and 31.0 mg of 1,1′-ferrocenedicarboxaldehyde (**1**). m.p. 252 °C; IR (cm^{-1}) 3059, 2924, 2216, 1617, 1593, 1456, 1421, 1324, 1255, 1157, 1111, 1070, 1000, 925, 824, 729, 667, 642, 621, 584, 477, 421; ^{1}H NMR spectra ($CDCl_3$) 7.40 (8H, q, *J* 5 Hz, ArH), 7.31 (2H, s, CH), 5.12 (4H, s, C_5H_4), 4.62 (4H, s, C_5H_4); ^{13}C NMR spectra ($CDCl_3$) 141.4, 125.9, 124.8, 107.3, 79.1, 77.2, 73.1, 72.9; HR-MS ($C_{30}H_{18}F_6FeN_2$) ES: $[M]^+$ *m/z* Calcd 576.0724, found 576.0717.

4.2.3. Synthesis of 1,1′-ferrocenyldi[-2(4-chlorophenyl)acrylonitrile] (4) and ferrocenyl-carboxl-2(4-chlorophenyl)acrylonitrile (5). The general procedure described in Section 4.2 was followed by using 1,1′-ferrocenyl-dicarboxaldehyde (**1**) (145.0 mg, 0.60 mM) and 4-chlorophenylacetonitrile (200.0 mg, 1.32 mM). Upon grinding the two substances in the presence of piperidine, the mixture formed a brown paste, which eventually turned red. Reaction completion was monitored using preparative TLC plates with a solvent system of hexane/dichloromethane (1 : 1). The red paste was dried, then purified by column chromatography in hexane and dichloromethane (1 : 1) to obtain two fractions of red solids (R_f = 0.5 and 0.375) and 87.0 mg of 1,1′-ferrocenedicarboxaldehyde (**1**). Characterization of the solid obtained from the less polar fraction (R_f = 0.5) gave **4** (153.0 mg, 52%) m.p. 238 °C; IR (cm^{-1}) 3087, 3050, 2209, 1898, 1649, 1598, 1493, 1456, 1411, 1374, 1329, 1305, 1251, 1186, 1094, 1037, 997, 917, 827, 815, 774, 745, 540, 499, 489, 437, 396; ^{1}H NMR spectra ($CDCl_3$) 7.22 (4H, s, ArH), 7.18 (4H, s, ArH), 7.15 (2H, s, CH), 5.06 (4H, s, C_5H_4), 4.56 (4H, s, C_5H_4); ^{13}C NMR spectra ($CDCl_3$) 140.1, 129.1, 126.0, 79.3, 72.7, 71.5; HR-MS ($C_{28}H_{18}Cl_2FeN_2$) ES: $[M]^+$ *m/z* Calcd 508.0196, found 508.0199.

Characterization of the solid obtained from the more polar fraction (R_f = 0.375) gave **5** (22.0 mg, 10%) m.p. 138 °C; IR (cm^{-1}) 3096, 2925, 2851, 2211, 1680, 1663, 1599, 1509, 1492, 1455, 1407, 1368, 1243, 1184, 1094, 1036, 1013, 997, 921, 825, 741, 485, 410; ^{1}H NMR spectra ($CDCl_3$) 9.93 (H, s, CHO), 7.54 (2H, d, *J* 8.4 Hz, ArH), 7.38 (2H, d, *J* 8.4 Hz, ArH), 7.18 (H, s, CH), 5.03 (2H, s, C_5H_4), 4.84 (2H, s, C_5H_4), 4.62 (2H, s, C_5H_4), 4.57 (2H, s, C_5H_4); ^{13}C NMR spectra ($CDCl_3$) 193.3, 141.4, 134.8, 132.7, 129.4, 127.4, 126.7, 118.3, 108.3, 80.3, 78.8, 74.5, 72.7, 72.5, 71.2, 71.2, 71.1; HR-MS ($C_{20}H_{14}OClFeN$) ES: $[M + H^+]$ *m/z* Calcd 376.0192, found 376.0180.

4.2.4. Synthesis of 1,1′-ferrocenyldi[-2(4-fluorophenyl)acrylonitrile] (6) and ferrocenyl-carboxl-2(4-fluorophenyl)acrylonitrile (7). The general procedure described in Section 4.2 was followed by using 1,1′-ferrocenyl-dicarboxaldehyde (**1**) (145.0 mg, 0.60 mM) and 4-fluorophenylacetonitrile (178.0 mg, 1.32 mM). Upon grinding, a red solution was formed which gradually turned into a reddish-brown solid. Reaction completion was monitored using preparative TLC plates with a solvent system of hexane/dichloromethane (1 : 1) and the product was then purified by column chromatography with a solvent system of hexane/diethyl ether (1 : 1) to obtain two fractions (R_f = 0.25 and 0.125) and 100.0 mg of 1,1′-ferrocenedicarboxaldehyde (**1**). The less polar fraction was isolated as a reddish-brown solid while the more polar fraction was isolated as a red solid. Characterization of the solid obtained from the less polar fraction (R_f = 0.25) gave **6** (20.0 mg, 7%) m.p. 214 °C; IR (cm^{-1}) 3052, 2921, 2851, 2212, 1604, 1593, 1510, 1456, 1418, 1372, 1311, 1281, 1265, 1236, 1163, 1107, 913, 814, 760, 725, 650, 594, 510, 480, 447, 426, 388; ^{1}H NMR spectra ($CDCl_3$) 7.32 (4H, q, *J* 3.5 Hz, ArH), 6.92 (4H, t, *J* 8.48 Hz, ArH), 7.13 (2H,s, CH), 5.03 (4H, s, C_5H_4), 4.56 (4H, s, C_5H_4); ^{13}C NMR spectra ($CDCl_3$) 139.9, 129.8, 126.7, 126.7, 118.6, 116.0, 115.8, 107.6, 79.4, 72.6, 71.4; HR-MS ($C_{28}H_{18}F_2FeN_2$) ES: $[M]^+$ *m/z* Calcd 476.0787, found 476.0789.

Characterization of the solid obtained from the less more polar fraction (R_f = 0.125) gave **7** (51.0 mg, 24%) m.p. 115 °C; IR (cm^{-1}) 3087, 2920, 2850, 2213, 1680, 1662, 1602, 1591, 1508, 1454, 1413, 1367, 1265, 1233, 1163, 1103, 1034, 1000, 921, 833, 763, 742, 651, 616, 593, 489, 445, 427, 398; ^{1}H NMR spectra ($CDCl_3$) 9.93 (H, s, CHO) 7.59 (2H, s, ArH), 7.12 (2H, s, ArH), 7.10 (H, s, CH), 5.03 (2H, s, C_5H_4), 4.84 (2H, s, C_5H_4), 4.62 (2H, s, C_5H_4),

4.56 (2H, s, C_5H_4); ^{13}C NMR spectra ($CDCl_3$) 193.3, 140.8, 130.4, 127.3, 127.3, 118.5, 116.3, 116.0, 108.5, 79.0, 72.5, 71.1; HR-MS ($C_{20}H_{14}$ OF_1FeN) ES: $[M]^+$ *m/z* Calcd 359.0409, found 359.0412.

4.3. *Reactions of ferrocenemonocarboxaldehyde (8) and phenylenediacetonitrile*

Ferrocenemonocarboxaldehyde (**8**) (400 mg, 1.86 mM) and phenylenediacetonitrile (203 mg, 1.30 mM) were added into a Pyrex tube fitted with a ground glass joint. The mixture was thoroughly ground with a glass rod in the presence of one to two drops of piperidine. A deep red gum formed which turned into a melt upon further grinding. The Pyrex tube was sealed and placed in a shaker for 20 min. The sample was subsequently dried in air followed by high vacuum drying to obtain a red solid. The reaction completion was monitored using preparative TLC plates with a solvent system of hexane/diethyl ether (3 : 2) and the product was then purified by column chromatography with a solvent system of hexane/diethyl ether (3 : 2) to obtain a major and a minor product and 58 mg of starting ferrocenemonocarboxaldehyde (**8**). The major product ($R_f = 0.325$) was isolated as red crystals and identified as phenylene-3,3′-*bis*-(ferrocenyl)-diacrylonitrile, **9**. The minor product ($R_f = 0.1$) was isolated as reddish-orange crystals and identified as 3-ferrocenyl-2(acetonitrophenyl) acrylonitrile **10**. Further characterization of **9** gave (319.0 mg, 65%); d.p. ca. 275 °C; IR (cm^{-1}) 3107, 2212, 1594, 1457, 1408, 1363, 1275, 1249, 1106, 1033, 997, 889, 837, 813, 721, 689, 507, 482, 463,448; ^1H NMR spectra ($CDCl_3$) 7.62 (4H, s, ArH), 7.43 (2H,s, CH), 4.98 (4H, s, C_5H_4), 4.56 (4H, s, C_5H_4), 4.23 (10H, s, C_5H_5); ^{13}C NMR spectra ($CDCl_3$) 143.6, 134.5, 125.6, 118.9, 105.8, 77.2, 71.9, 70.3, 69.9; HR-MS ($C_{32}H_{24}Fe_2N_2$) ES: $[M]^+$ *m/z* Calcd 548.0638, found 548.0641.

Further characterization of **10** gave (152.0 mg, 30%) m.p. 151 °C; IR (cm^{-1}) 3094, 2934, 2212, 1919, 1783, 1594, 1515, 1456, 1408, 1361, 1320, 1268, 1249, 1191, 1104, 1049, 1032, 997, 915, 837, 813, 722, 690, 613, 481, 449, 429; ^1H NMR spectra ($CDCl_3$) 7.61 (2H, s, ArH), 7.59 (2H, s, ArH), 7.37 (1H, s, CH), 4.96 (2H, t, *J* 1.7 Hz, C_5H_4), 4.54 (2H, t, *J* 1.8 Hz, C_5H_4), 4.23 (5H, s, C_5H_4), 3.75 (2H, s, CH_2) ^{13}C NMR spectra ($CDCl_3$) 144.0, 134.8, 129.8, 128.6, 125.8, 118.9, 117.4, 105.6, 77.2, 71.8, 70.3, 69.9, 23.4; *m/z;* $[M^+]$, 352.1 HR-MS ($C_{21}H_{16}FeN_2$) ES: $[M]^+$ *m/z* Calcd 352.0663, found 352.0671.

5. X-ray crystallography

5.1. *Structural analysis of 2, 4, 9, and 10*

Data for X-ray diffraction of **2**, **4**, **9**, and **10** were collected from APEX [38] with cell refinement of SAINT-Plus [38]. The data reduction was done by using SAINT-Plus and XPREP [38] while the structures were solved by direct methods with SHELXS9 [39] program(s). The structures obtained were refined by using SHELXL97 [39] and their molecular graphics were obtained by using ORTEP-3 [40]. The software *WinGX* was used to prepare material for publication [41]. The crystal data and structure refinement for **2**, **4**, **9**, and **10** are summarized in table 8.

Table 8. Crystallographic data and structure refinements for **2**, **4**, **9**, and **10**.

Parameter	**2**	**4**	**9**	**10**
Empirical formula	$C_{30}H_{18}Fe_1N_4$	$C_{28}H_{18}Fe_1N_2$	$C_{32}H_{24}Fe_2N_2$	$C_{21}H_{16}Fe_1N_2$
Formula weight	490.33	509.19	548.23	352.21
Temperature (K)	173(2)	173(2)	173(2)	173(2)
Wavelength (Å)	0.71073	0.71073	0.71073	0.71073
Crystal system	Monoclinic	Monoclinic	Monoclinic	Triclinic
Space group	$P2_1/c$	$P2_1/c$	$P2_1/c$	$P\bar{1}$
Unit-cell dimensions (Å/°)				
a, *α*	7.3307(4)	7.2041(5)	11.4369(3)	7.2547(3), 101.730(2)
b, *β*	25.1890(14), 119.733(3)	23.4176(14), 108.902(4)	28.7450(7), 93.6830(10)	11.9787(5), 92.658(2)
c, *γ*	13.8031(7)	13.4176(8)	7.5275(2)	19.2512(9), 90.818(2)
V (Å^3)	2213.2(2)	2149.4(2)	2469.58(11)	1635.78(12)
Z	4	4	4	4
σ (mg/m^3)	1.472	1.574	1.475	1.430
μ (mm^{-1})	0.709	0.971	1.199	0.924
F (000)	1008	1040	1128	728
Crystal size (mm)	0.38 × 0.26 × 0.08	0.35 × 0.28 × 0.12	0.49 × 0.47 × 0.10	0.43 × 0.28 × 0.09
θ range (°)	1.88 → 25.00	1.74 → 26.13	1.78 → 28.34	1.08 → 28.00
Index ranges	−8 → 8	−8 → 8	−14 → 15	−9 → 9
	−29 → 29	−28 → 28	−38 → 38	−15 → 15
	−16 → 16	−15 → 14	−10 → 10	−25 → 25
Reflections	33,106	15,565	75,646	49,618
Indep. reflections	3786[R_{int} = 0.0335]	3829 [R_{int} = 0.0302]	6131 [R_{int} = 0.0366]	7796[R_{int} = 0.0292]
Completeness to *θ* % (°)	96.9 (25.00)	89.5 (26.13)	99.5 (28.34)	98.5 (28.00)
Absorption correction	Semi-empirical from equivalents	Semi-empirical from equivalents	Semi-empirical from equivalents	Semi-empirical from equivalents
Max and min trans.	0.9454 and 0.7743	0.8924 and 0.7274	0.8895 and 0.5911	0.9214 and 06,919
Refinement	Full-matrix least-squares on F^2	Full-matrix least-squares on F^2	Full-matrix least-squares on F^2	Full-matrix least-squares on F^2
Data/restraints/parameters	3786/0/316	3829/0/298	6131/0/325	7796/0/434
Goof on F^2	1.008	1.238	1.121	1.071
Final R indices	R_1 = 0.0296,	R_1 = 0.0572,	R_1 = 0.0316,	R_1 = 0.0593,
[$I > 2$ sigma(I)]	wR_2 = 0.0779	wR_2 = 0.1333	wR_2 = 0.0806	wR_2 = 0.1867
R indices (all data)	R_1 = 0.0364,	R_1 = 0.0595,	R_1 = 0.0398,	R_1 = 0.0663,
	wR_2 = 0.0814	wR_2 = 0.1343	wR_2 = 0.0845	wR_2 = 0.1913
Largest diff. peak and hole (e Å^3)	0.339 and −0.339	2.298 and −0.712	0.452 and −0.537	1.758 and −0.660

Supplementary material

Tables and figures giving ^{1}H and ^{13}C NMR spectra, IR spectra, and HR-MS analysis for **2**, **3**, **4**, **5**, **6**, **7**, **9**, and **10**. UV–visible spectrophotometric and cyclic voltammetric data for **2**, **3**, **4**, **9**, and **10**. CIF files and crystallographic data of **2**, **4**, **9**, and **10**. Responses to the various alerts from CIF validation are provided in the CIF files under the publication section, experimental refinement section.

Acknowledgements

This research was financed by the National Research Foundation (NRF) and the University of KwaZulu-Natal (UKZN). Lucy M. Ombaka thanks the UKZN College of Agriculture, Engineering and Science for the award of a postgraduate bursary. We are also grateful to Prof. B.S. Martincigh, Dr R.S. Mwakubambanya, Godfrey Keru, and Mombeshora Tonde for their critical comments on the manuscript.

References

[1] M. Himaja, P. Das, A. Karigar. *Int. J. Res. Ayurveda Pharm.*, **4**, 1079 (2011).
[2] D. Braga, S.L. Giaffreda, F. Grepioni, A. Pettersen, L. Maini, M. Curzi, M. Polito. *Dalton Trans.*, 1249 (2006).
[3] A. McCluskey, P.J. Robinson, T. Hill, J.L. Scott, J.K. Edwards. *Tetrahedron Lett.*, **43**, 3117 (2002).
[4] A. Majumder, R. Gupta, A. Jain. *Green Chem. Lett. Rev.*, **6**, 151 (2013).
[5] O. Galangau, I. Fabre-Francke, S. Munteanu, C. Dumas-Verdes, G. Clavier, R. Méallet-Renault, R.B. Pansu, F. Hartl, F. Miomandre. *Electrochim. Acta*, **87**, 809 (2013).
[6] S. Venkatraman, R. Kumar, J. Sankar, T.K. Chandrashekar, K. Sendhil, C. Vijayan, A. Kelling, M.O. Senge. *Chem. Eur. J.*, **10**, 1423 (2004).
[7] O.F. Mohammed, A.A.O. Sarhan. *Chem. Phys.*, **372**, 17 (2010).
[8] P. Camurlu, Z. Bicil, C. Gültekin, N. Karagoren. *Electrochim. Acta*, **63**, 245 (2012).
[9] S. Braga, A.M.S. Silva. *Organometallics*, **32**, 5626 (2013).
[10] V.O. Nyamori, S.D. Mhlanga, N.J. Coville. *J. Organomet. Chem.*, **693**, 2205 (2008).
[11] R.S. Oosthuizen, V.O. Nyamori. *Appl. Organomet. Chem.*, **26**, 536 (2012).
[12] E.N. Nxumalo, N.J. Coville. *Materials*, **3**, 2141 (2010).
[13] E.N. Nxumalo, V.P. Chabalala, V.O. Nyamori, M.J. Witcomb, N.J. Coville. *J. Organomet. Chem.*, **695**, 1451 (2010).
[14] M.I. Ionescu, Y. Zhang, R. Li, H. Abou-Rachid, X. Sun. *Appl. Surf. Sci.*, **258**, 4563 (2012).
[15] C. Imrie, P. Kleyi, V.O. Nyamori, T.I.A. Gerber, D.C. Levendis, J. Look. *J. Organomet. Chem.*, **692**, 3443 (2007).
[16] C. Imrie, V.O. Nyamori, T.I.A. Gerber. *J. Organomet. Chem.*, **689**, 1617 (2004).
[17] W. Liu, Q. Xu, Y. Ma, Y. Liang, N. Dong, D. Guan. *J. Organomet. Chem.*, **625**, 128 (2001).
[18] P.E. Kleyi, C.W. McCleland, T.I.A. Gerber. *Polyhedron*, **29**, 1095 (2010).
[19] S. Yuan, Z. Li, L. Xu. *Res. Chem. Intermed.*, **38**, 393 (2012).
[20] A. González, P. Vázquez, T. Torres. *Tetrahedron Lett.*, **40**, 3263 (1999).
[21] N. Dwadnia, F. Allouch, N. Pirio, J. Roger, H. Cattey, S. Fournier, M.-J. Penouilh, C.H. Devillers, D. Lucas, D. Naoufal, R.B. Salem, J.-C. Hierso. *Organometallics*, **32**, 5784 (2013).
[22] P.Y. Bruice. *Organic Chemistry*, 5th Edn, pp. 683–686, Pearson Education, Upper Sadle River (2007).
[23] D. Braga, M. Polito, D. D'Addario, E. Tagliavini, D.M. Proserpio, F. Grepioni, J.W. Steed. *Organometallics*, **22**, 4532 (2003).
[24] Y. Yamaguchi, W. Ding, C.T. Sanderson, M.L. Borden, M.J. Morgan, C. Kutal. *Coord. Chem. Rev.*, **251**, 515 (2007).
[25] B. Dhokale, P. Gautam, R. Misra. *Tetrahedron Lett.*, **53**, 2352 (2012).
[26] K. Yoshiharu, M. Takashi, M. Shuichi. In *Optical recording materials sensitive to blue laser beam, publication number, 2002-002110, Patent abstracts of Japan, Kokai Tokyo Koho*, pp. 13 (2002).
[27] O.F. Mohammed, E. Vauthey. *J. Phys. Chem. A*, **112**, 5804 (2008).

[28] P. Kaur, M. Kaur, G. Depotter, S. Van Cleuvenbergen, I. Asselberghs, K. Clays, K. Singh. *J. Mater. Chem.*, **22**, 10597 (2012).
[29] W.E. Geiger, N.G. Connelly. *Chem. Rev.*, **96**, 877 (1996).
[30] V. Lakshmi, G. Santosh, M. Ravikanth. *J. Organomet. Chem.*, **696**, 925 (2011).
[31] R.S. Bayly, P.D. Beer, G.Z. Chen. In *Ferrocene Ligands, Materials and Biomolecules*, P. Štěpnička (Ed.), pp. 281–318, John Wiley & Sons, Atrium Southern Gate, Chichester (2008).
[32] L.V. Snegur, A.A. Simenel, Y.S. Nekrasov, E.A. Morozova, Z.A. Starikova, S.M. Peregudova, Y.V. Kuzmenko, V.N. Babin, L.A. Ostrovskaya, N.V. Bluchterova, M.M. Fomina. *J. Organomet. Chem.*, **689**, 2473 (2004).
[33] S. Barlowa, S.R. Marder. *Chem. Commun.*, 1555, (2000).
[34] S.M. Batterjee, M.I. Marzouk, M.E. Aazab, M.A. El-Hashash. *Appl. Organomet. Chem.*, **17**, 291 (2003).
[35] F. Cozzi, J.S. Siegel. *Pure Appl. Chem.*, **67**, 683 (1995).
[36] V.O. Nyamori, G. Keru, B. Omondi. *Acta Crystallogr. Sect. E: Struct. Rep. Online*, **68**, m1535 (2012).
[37] D. Onyancha, V. Nyamori, C.W. McCleland, C. Imrie, T.I.A. Gerber. *J. Organomet. Chem.*, **694**, 207 (2009).
[38] Bruker. *APEX2, SAINT-Plus, XPREP and SADABS*, Bruker AXS Inc., Madison, WI (2008).
[39] G.M. Sheldrick. *Acta Crystallogr.*, **A64**, 112 (2008).
[40] L.J. Farrugia. *J. Appl. Crystallogr.*, **30**, 565 (1997).
[41] L.J. Farrugia. *J. Appl. Crystallogr.*, **32**, 837 (1999).